Chapter 3

Fractal Fracture Mechanics Applied to Materials Engineering

Lucas Máximo Alves and Luiz Alkimin de Lacerda

Additional information is available at the end of the chapter

http://dx.doi.org/10.5772/52511

1. Introduction

The Classical Fracture Mechanics (CFM) quantifies velocity and energy dissipation of a crack growth in terms of the projected lengths and areas along the growth direction. However, in the fracture phenomenon, as in nature, geometrical forms are normally irregular and not easily characterized with regular forms of Euclidean geometry. As an example of this limitation, there is the problem of stable crack growth, characterized by the *J-R* curve [1, 2]. The rising of this curve has been analyzed by qualitative arguments [1, 2, 3, 4] but no definite explanation in the realm of EPFM has been provided.

Alternatively, fractal geometry is a powerful mathematical tool to describe irregular and complex geometric structures, such as fracture surfaces [5, 6]. It is well known from experimental observations that cracks and fracture surfaces are statistical fractal objects [7, 8, 9]. In this sense, knowing how to calculate their true lengths and areas allows a more realistic mathematical description of the fracture phenomenon [10]. Also, the different geometric details contained in the fracture surface tell the history of the crack growth and the difficulties encountered during the fracture process [11]. For this reason, it is reasonable to consider in an explicit manner the fractal properties of fracture surfaces, and many scientists have worked on the characterization of the topography of the fracture surface using the fractal dimension [12, 13]. At certain point, it became necessary to include the topology of the fracture surface into the equations of the Classical Fracture Mechanics theory [6, 8, 14]. This new "Fractal Fracture Mechanics" (FFM) follows the fundamental basis of the Classical Fracture Mechanics, with subtle modifications of its equations and considering the fractal aspects of the fracture surface with analytical expressions [15, 16].

The objective of this chapter is to include the fractal theory into the elastic and plastic energy released rates G_0 and J_0, in a different way compared to other authors [8, 13, 14, 17, 18, 19]. The non-differentiability of the fractal functions is avoided by developing a differentiable

analytic function for the rugged crack length [20]. The proposed procedure changes the classical G_0, which is linear with the fracture length, into a non-linear equation. Also, the same approach is extended and applied to the Eshelby-Rice non-linear *J*-integral. The new equations reproduce accurately the growth process of cracks in brittle and ductile materials. Through algebraic manipulations, the energetics of the geometric part of the fracture process in the *J*-integral are separated to explain the registered history of strains left on the fracture surfaces. Also, the micro and macroscopic parts of the *J*-integral are distinguished. A generalization for the fracture resistance *J-R* curve for different materials is presented, dependent only on the material properties and the geometry of the fractured surface.

Finally, it is shown how the proposed model can contribute to a better understanding of certain aspects of the standard ASTM test [15].

2. Literature review of fractal fracture mechanics

2.1. Background of the fractal theory in fracture mechanics

Mandelbrot [21] was the first to point out that cracks and fracture surfaces could be described by fractal models. Mecholsky *et al*. [12] and Passoja and Amborski [22] performed one of the first experimental works reported in the literature, using fractal geometry to describe the fracture surfaces. They sought a correlation of the roughness of these surfaces with the basic quantity D called fractal dimension.

Since the pioneering work of Mandelbrot *et al.* [23], there have been many investigations concerning the fractality of crack surfaces and the fracture mechanics theory. They analyzed fracture surfaces in steel obtained by Charpy impact tests and used the "slit island analysis" method to estimate their fractal dimensions. They have also shown that D was related to the toughness in ductile materials.

Mecholsky *et al.* [12, 24] worked with brittle materials such as ceramics and glass-ceramics, breaking them with a standard three point bending test. They calculated the fractal dimension of the fractured surfaces using Fourier spectral analysis and the "slit island" method, and concluded that the brittle fracture process is a self-similar fractal.

It is known that the roughness of the fracture surface is related to the difficulty in crack growth [25] and several authors attempted to relate the fractal dimension with the surface energy and fracture toughness. Mecholsky *et al.* [24] followed this idea and suggested the dependence between fracture toughness and fractal dimension through

$$K_{IC} = E\left(D^* a_0\right)^{1/2} \tag{1}$$

where *E* is the elastic modulus of the material, a_0 is its lattice parameter, $D^* = D - d$ is the fractional part of the fractal dimension and *d* is the Euclidean projection dimension of the fracture.

Mu and Lung [26] suggested an alternative equation, a power law mathematical relation between the surface energy and the fractal dimension. It will be seen later in this chapter that both suggestions are complementary and are covered by the model proposed in this work.

2.2. The elasto-plastic fracture mechanics

There have been several proposals for including the fractal theory into de fracture mechanics in the last three decades. Williford [17] proposed a relationship between fractal geometric parameters and parameters measured in fatigue tests. Using Williford's proposal Gong and Lai [27] developed one of the first mathematical relationships between the *J-R* curve and the fractal geometric parameters of the fracture surface. Mosolov and Borodich [32] established mathematical relations between the elastic stress field around the crack and the rugged exponent of the fracture surface. Later, Borodich [8, 29] introduced the concept of specific energy for a fractal measurement unit. Carpinteri and Chiaia [30] described the behavior of the fracture resistance as a consequence of its self-similar fractal topology. They used Griffith's theory and found a relationship between the *G*-curve and the advancing crack length and the fractal exponent. Despite the non-differentiability of the fractal functions, they were able to obtain this relationship through a renormalizing method. Bouchaud and Bouchaud [31] also proposed a formulation to correlate fractal parameters of the fracture surface.

Yavari [28] studied the *J*-integral for a fractal crack and showed that it is path-dependent. He conjectured that a *J*-integral fractal should be the rate of release of potential energy per unit of measurement of the fractal crack growth.

Recently, Alves [16] and Alves *et al.* [20] presented a self-affine fractal model, capable of describing fundamental geometric properties of fracture surfaces, including the local and global ruggedness in Griffith´s criterion. In their formulations the fractal theory was introduced in an analytical context in order to establish a mathematical expression for the fracture resistance curve, putting in evidence the influence of the crack ruggedness.

3. Postulates of a fracture mechanics with irregularities

To adapt the CFM, starting from the smooth crack path equations to the rugged surface equations, and using the fractal geometry, it is necessary to establish in the form of postulates the assumptions that underlie the FFM and its correspondence with the CFM.

I. Admissible fracture surfaces

Consider a crack growing along the x-axis direction (Figure 1), deviating from the x-axis path by floating in y-direction. The trajectory of the crack is an admissible fractal if and only if it represents a single-valued function of the independent variable x.

II. Scale limits for a fractal equivalence of a crack

The irregularities of crack surfaces in contrast to mathematical fractals are finite. Therefore, the crack profiles can be assumed as fractals only in a limited scale $l_0 \le L_0 \le L_{0\max}$ [36]. The

lower limit l_0 is related to the micro-mechanics of the cracked material and the upper limit $L_{0\max}$ is a function of the geometric size of the body, crack length and other factors.

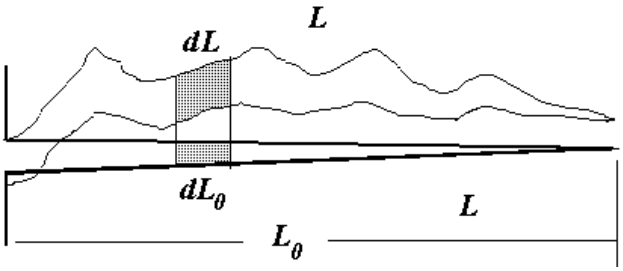

Figure 1. Rugged crack and its projection in the plan of energetic equivalence.

III. Energy equivalence between the rugged crack surface and its projection

Irwin *apud* Cherepanov *et al.* [36] realized the mathematical complexity of describing the fracture phenomena in terms of the complex geometry of the fracture surface roughness in different materials. For this reason, he proposed an energy equivalence between the rough surface path and its projection on the Euclidean plane.

In the energetic equivalence between rugged and projected crack surfaces it is considered that changes in the elastic strain energy introduced by a crack are the same for both rugged and projected paths,

$$U_{L0} = U_L \tag{2}$$

where the subscript " 0 " denotes quantities in the projected plane. Consequently, the surface energy expended to form rugged fracture surfaces or projected surfaces are also equivalent,

$$U_{\gamma 0} = U_\gamma \tag{3}$$

IV. Invariance of the equations

Consider a crack of length L and the quantities that describe it. Assuming the existence of a geometric operation that transforms the real crack size L to an apparent projected size L_0, the length L may be described in terms of L_0 by a fractal scaling equation, as presented in a previous chapter.

It is claimed that the classical equations of the fracture mechanics can be applied to both rugged and projected crack paths, i.e., they are invariant under a geometric transformation between the rugged and the projected paths. In the crack wrinkling operation (smooth to rough) it is desired to know what will be the form of the fracture mechanics equations for the rough path as a function of the projected length L_0, and their behavior for different roughness degrees and observation scales.

V. Continuity of functions

It is considered that the scalar and vector functions that define the irregular surfaces $\vec{A} = \vec{A}(x,y)$ are described by a model (as the fractal model) capable of providing analytical and differentiable functions in the vicinity of the generic coordinate points $P = P(x,y,z)$, so that it is possible to calculate the surface *roughness*. Thus, it is always possible to define a normal vector in corners.

VI. Transformations from the projected to rugged path equations

As a consequence of the previous two postulates, it can be shown using the chain rule that the relationship between the rates for projected and rugged paths are given by

$$\frac{df(L_0)}{dL_0} = \frac{df(L)}{dL}\frac{dL}{dL_0} \tag{4}$$

This result is used to transform the equations from the rugged to the projected path.

4. Energies in linear elastic fracture mechanics for irregular media

The study of smooth, rough, fractal and non-fractal cracks in Fracture Mechanics requires the development of their respective equations of strain and surface energies.

4.1. The elastic strain energy U_L for smooth, rugged and fractal cracks

Consider three identical plates of thickness t, with Young's modulus E', subjected to a stress σ, each of them cracked at its center with a smooth, a rugged and a fractal crack as shown in Figure 2. The area of the unloaded elastic energy due to the introduction of the crack with length L_l is

$$A_l = m_l L_l^2 \tag{5}$$

where $m_l = \pi$ is the shape factor for the smooth crack. The accumulated elastic energy is

$$\Delta U_e = \int \frac{\sigma^2}{2E'} dV \tag{6}$$

Thus, the elastic energy released by the introduction of a smooth crack with length L_l is

$$\Delta U_l = -m_l t \frac{\sigma_l^2 L_l^2}{2E'_l} \tag{7}$$

For an elliptical crack the unloaded region can be considered almost elliptical and the shape factor is $m_l = \pi$, thus

$$\Delta U_l = -t\frac{\pi\sigma_l^2 L_l^2}{2E'_l} \tag{8}$$

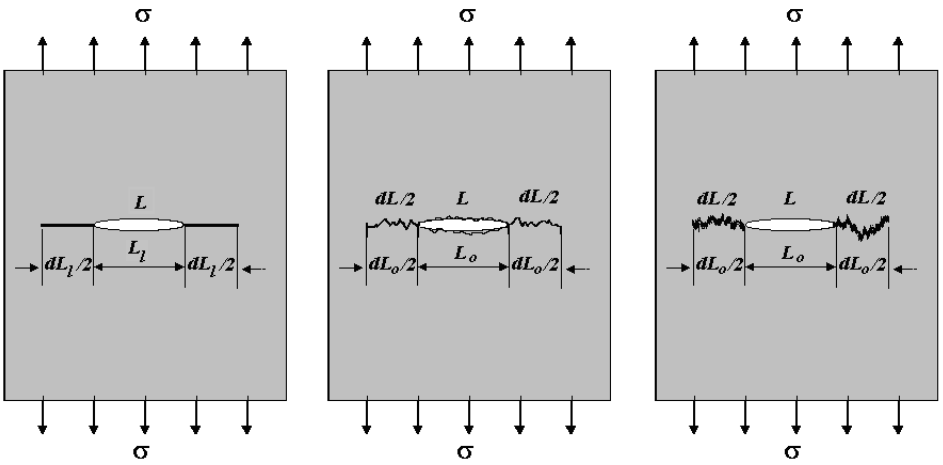

Figure 2. Griffith model for the crack growth introduced in a plate under σ stress: a) flat crack and initial length L_l with increase dL_l in size; b) rugged crack and initial length L with increase dL in size; c) fractal crack, showing increase dL in size.

Analogously, the area of the unloaded elastic energy due to the introduction of a rugged crack of length L is given by

$$A = m^* L^2 \tag{9}$$

where m^* is a shape factor for the rugged crack. Thus, the elastic energy released by the introduction of a rugged crack with length L is

$$\Delta U_L = -m^* t\frac{\sigma_r^2 L^2}{2E'} \tag{10}$$

Considering that the rugged crack is slightly larger than its projection, then

$$L = \varsigma L_0 \tag{11}$$

Consequently, the change of elastic strain energy from the point of view of the projected length L_0 can be expressed as:

$$\Delta U_{L0} = -m^* t\frac{\sigma_0^2 L_0^2}{2E'} \tag{12}$$

where $\sigma_0 = \sigma_r\varsigma$.

4.2. A self-affine fractal model for a crack - LEFM

To take the roughness into account, it will be inserted in the CFM equations a self-affine fractal model developed in a previous chapter of this book.

4.2.1. The relationship between strain energies for rugged U_L and projected U_{L0} cracks in terms of fractal geometry

The crack length of the self-affine fractal can be expressed as

$$L = L_0\sqrt{1+\left(\frac{H_0}{l_0}\right)^2\left(\frac{L_0}{l_0}\right)^{2(H-1)}} \tag{13}$$

where H_0 is the vertically projected crack length and the unloading fractal area of the elastic energy can be expressed as a function of the apparent length,

$$A_0 = m_0 {L_0}^2 \tag{14}$$

And results that

$$\Delta U_{L0} = 2m^* t\int \frac{{\sigma_r}^2}{2{E'}_0}\left(1+(2-H)\left(\frac{H_0}{l_0}\right)^2\left(\frac{l_0}{L_0}\right)^{2H-2}\right)L_0 dL_0 \tag{15}$$

Therefore, the elastic energy released by the introduction of a crack length L_0 is

$$\Delta U_{L0} = -m^* t\frac{{\sigma_0}^2{L_0}^2}{2{E'}_0} \tag{16}$$

where $\sigma_0 = \sigma_r\sqrt{1+\left(\frac{H_0}{l_0}\right)^2\left(\frac{l_0}{L_0}\right)^{2H-2}}$

Observe that equation (12) is recovered from equation (16) applying the limits $H_0 \to l_0 \ll L_0$ and $H \to 1.0$ with $\sigma_r = \sigma_0$ and $E' = {E'}_0$.

To understand the effect of crack roughness on the change of elastic strain energy, one may consider postulates III and IV, thus

$$\Delta U_{Lo} = \Delta U_L = -\frac{m^*{\sigma_r}^2{L_0}^2}{2E'}\left[1+\left(\frac{H_0}{l_0}\right)^2\left(\frac{l_0}{L_0}\right)^{2H-2}\right] \tag{17}$$

It can be noticed that for $H \to 1$, which corresponds to a smoother surface, the relationship between the strain energy and the projected length L_0 is more linear. While for $H \to 0$,

which corresponds to a rougher surface, this relationship is increasingly non-linear. This is reasonable since the more ruggedness, more elastic strain per unit of crack length.

4.2.2. Relationship between the applied stress on the rough and projected crack lengths

Comparing (8), (10) and (12), one has

$$\Delta U_{L0} = \Delta U_{Ll}\left(\frac{m^*}{\pi}\right) = \Delta U_L \tag{18}$$

Then, from postulate III, i.e., the following relationship is valid only for the situation of free loading without crack growth.

$$\frac{\sigma_0^{\,2}}{E'_0} = \frac{\sigma_r^{\,2}}{E'}\left(\frac{L}{L_0}\right)^2 \tag{19}$$

Using equation (13) in (19), one has the resilience as a function of the projected length L_0

$$\frac{\sigma_0^{\,2}}{E_0} = \frac{1}{\sqrt{2}}\frac{\sigma^2}{E}\left[1+\left(\frac{H_0}{l_0}\right)^2\left(\frac{l_0}{L_0}\right)^{2H-2}\right] \tag{20}$$

Or, the rugged length L can be written in terms of the projected length L_0, thus

$$L = \sqrt{\frac{E'}{E'_0}}\left(\frac{\sigma_0}{\sigma_r}\right)L_0 \tag{21}$$

Since the elasticity modulus is independent of the crack path, one has

$$\sigma_0 L_0 = \sigma_r L \tag{22}$$

Substituting equation (13) in equation (22), one has the relationship between stresses on the rough and projected surfaces,

$$\sigma_0 = \frac{\sigma_r}{\sqrt{2}}\left[1+\left(\frac{H_0}{l_0}\right)^2\left(\frac{l_0}{L_0}\right)^{2H-2}\right]^{1/2} \tag{23}$$

This last result is still incomplete since it is not valid for crack propagation. For its correction it will be considered that the elastic energy released rate G can be expressed as a function of G_0 according to equation (4).

4.2.3. The surface energy $U_{\gamma 0}$ for smooth, rugged and projected cracks in accordance with fractal geometry

The surface energy of a smooth and a rugged crack are, respectively, given by

$$\begin{aligned}\Delta U_{\gamma l} &= 2\left(L_l t\right)\gamma_l \\ \Delta U_{\gamma l} &= 2\gamma_l t L_l\end{aligned} \tag{24}$$

and

$$\begin{aligned}\Delta U_{\gamma L} &= 2\left(Lt\right)\gamma_r \\ \Delta U_{\gamma L} &= 2\gamma_r t L\end{aligned} \tag{25}$$

Using equation (11), the surface energy of the projected length L_0 is given by

$$\begin{aligned}\Delta U_{\gamma 0} &= 2\left(tL_0\right)\gamma_0 \\ \Delta U_{\gamma 0} &= 2\gamma_0 t L_0\end{aligned} \tag{26}$$

where $\gamma_0 = \gamma_r \varsigma$. The surface energy equation (25) can be rewritten in terms of the projected length L_0 of a self-affine fractal crack

$$\Delta U_{\gamma 0} = 2\gamma_r t L_0 \sqrt{1+\left(\frac{H_0}{l_0}\right)^2 \left(\frac{l_0}{L_0}\right)^{2H-2}} \tag{27}$$

To see the influence of crack roughness on the surface energy, one may consider postulates III and IV, thus

$$U_{\gamma 0} = U_\gamma = \frac{2\gamma_r L_0}{\sqrt{2}} \sqrt{1+\left(\frac{H_0}{l_0}\right)^2 \left(\frac{l_0}{L_0}\right)^{2H-2}} \tag{28}$$

5. Stable or quasi-static fracture mechanics to the rough path

In this section, a review of the conceptual changes introduced by Irwin (1957) in Griffith's theory (1920) is presented considering an irregular fracture surface, taking into account the postulates previously proposed. The purpose of this section is to use the mathematical formalism of Linear Elastic Fracture Mechanics for stable growth of smooth cracks, generalizing it to the case of an irregular rough crack.

5.1. The Griffith energy balance in terms of fractal geometry

According to Griffith´s energy balance, one has

$$dU_T = d\left(U_i + U_L - F + U_\gamma\right) \le 0 \tag{29}$$

whilst

$$F - U_L \ge U_\gamma \tag{30}$$

Where U_T is the total energy, U_i is the initial potential elastic energy, F is the work done by external forces, U_L is the change of elastic energy stored in the body caused by the introduction of the crack length L_0 and U_γ is the energy released to form the fracture surfaces.

One can now add the contributions of ΔU_{L0} and $\Delta U_{\gamma 0}$ to reproduce Griffith's energy balance in a fractal vision. In other words,

$$\Delta U_T = U_i + \Delta U_L + \Delta U_\gamma - F \tag{31}$$

and

$$\frac{d}{dL_l}(U_i + -\frac{\pi\sigma^2 {L_0}^2}{2E}\left[1+\left(\frac{H_0}{l_0}\right)^2\left(\frac{l_0}{L_0}\right)^{2H-2}\right] + \frac{2\gamma L_o}{\sqrt{2}}\sqrt{1+\left(\frac{H_0}{l_0}\right)^2\left(\frac{l_0}{L_0}\right)^{2H-2}} - F) \le 0 \tag{32}$$

This new result is shown in Figure 3, which is analogous to the traditional Griffith energy balance graphs, but distorted due to the roughness of the fracture surface. Observe that for a reference total energy value the roughness of the crack surface tends to increase the critical size of the fracture L_{0C} compared to a material with a smooth fracture $\left(L_{lC} \le L_C\right)$. This is due to the roughness being a result of the interaction of the crack with the microstructure of the material.

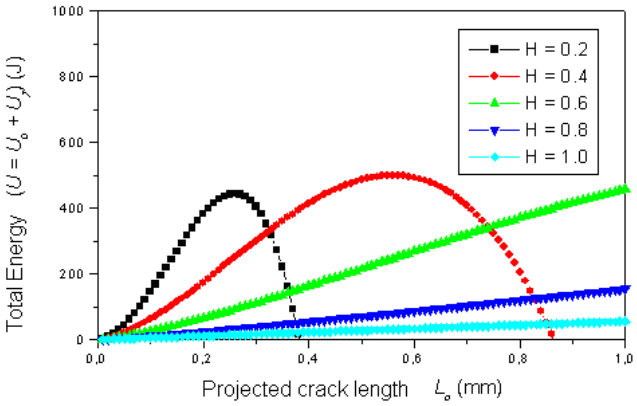

Figure 3. Griffith's energy balance in the view of the fractal geometry of fracture surface roughness.

5.2. The modification of Irwin in Griffith's energy balance theory for smooth, rugged and projected cracks

Irwin found from Griffith's instability equation, given by (29), that this instability should take place by varying the crack length, so

$$\frac{d}{dL}\left(U_i + U_L + U_\gamma - F\right) \le 0 \tag{33}$$

which can be rewritten as

$$\frac{d}{dL}(F - U_L) \ge \frac{dU_\gamma}{dL} \tag{34}$$

since U_i is constant. On the left hand side of equation (34), $dF/dL - dU_L/dL$ is the amount of energy that remains available to increase crack extension by an amount dL. On the right hand side of equation (34), dU_γ/dL is the surface energy that must be released to form the rugged crack surfaces. This energy is the crack growth resistance.

Deriving equation (30) with respect to the projected crack length L_0, one has

$$\frac{d}{dL_0}(F - U_L) \ge \frac{dU_\gamma}{dL_0} \tag{35}$$

Considering postulate II, one can apply the derivation chain rule and obtain

$$\frac{d}{dL}(F - U_L)\frac{dL}{dL_0} \ge \frac{dU_\gamma}{dL}\frac{dL}{dL_0} \tag{36}$$

Considering the following cases:

i. Fixed grips condition with $F = constant$: since $U_L = U_{L0} = -m^* \sigma^2 L_0^2/2E'$ decreases with the crack length, and using equations (10) and (25) in (36), one can derive

$$\frac{m^* {\sigma_r}^2 L}{E'} \ge 2\gamma_r. \tag{37}$$

Or, by using equations (17) and (26) in (35), one finds

$$\frac{m^* {\sigma_r}^2 L_0}{2E'}\left(1 + (2 - H)\left(\frac{H_0}{l_0}\right)^2\left(\frac{l_0}{L_0}\right)^{2H-2}\right) \ge 2\gamma_0. \tag{38}$$

ii. Condition of constant loading or stress, where necessarily $|F| = 2|U_L|$, since $U_L = U_{L0} = m^* \sigma^2 L_0^2/2E'$ increases with the work of external forces, and using equations (10) and (25) in (36), one can find

$$\frac{m^* {\sigma_r}^2 L}{E'} \ge 2\gamma_r. \tag{39}$$

Or, by using equations (17) and (26) in (35), one has

$$\frac{m^{*}\sigma_r^{\,2}L_0}{2E'}\left(1+(2-H)\left(\frac{H_0}{l_0}\right)^2\left(\frac{l_0}{L_0}\right)^{2H-2}\right)\geq 2\gamma_0. \tag{40}$$

Irwin defined the elastic energy released rate G and the fracture resistance R in equation (34), like

$$G\equiv\frac{d(F-U_L)}{dL} \tag{41}$$

and

$$R\equiv\frac{dU_\gamma}{dL}. \tag{42}$$

These definitions can be extended to the terms in equation (35), so

$$G_0\geq R_0 \qquad G_0\equiv\frac{d(F-U_{L0})}{dL_0} \tag{43}$$

and

$$R_0\equiv\frac{dU_{\gamma 0}}{dL_0}. \tag{44}$$

Notice that the proposal made by Irwin extended the concept of specific energy γ_{eff} to the concept of R-curve given by equation (42), allowing to consider situations where the microstructure of the material interacts with the crack tip. In this way, it is assumed that the surface energy is dependent on the direction of crack growth.

Finally, using equations (41) and (42) in (36), the Griffith-Irwin criterion is obtained,

$$G\frac{dL}{dL_0}\geq R\frac{dL}{dL_0}. \tag{45}$$

5.3. Comparative analysis between smooth, projected and rugged fracture quantities

Based on the results of the previous section, further analyses of the magnitudes of the Fracture Mechanics are performed in order to obtain a mathematical reformulation for an irregular or rugged Fracture Mechanics.

5.3.1. Relationship between the elastic energy released rate rates for smooth, projected and rugged cracks

Using the chain rule, it is possible to write G_0 in terms of G,

$$G_0 = G\frac{dL}{dL_0} \tag{46}$$

The energetics equivalence between the rugged surface and its projection establishes that the energy per unit length along the rugged path is equal to the energy per unit length along the projected path. Notice that

$$\frac{dU_{L0}}{dL_0} \geq \frac{dU_L}{dL} \tag{47}$$

since $dL/dL_0 \geq 1$, therefore,

$$G_0 \geq G. \tag{48}$$

The elastic energy released rates for the projected and rugged paths are, respectively

$$G_0 = \frac{dU_{L0}}{dL_0} = \frac{m^* \sigma_0{}^2 L_0}{E'_0} \tag{49}$$

and

$$G = \frac{dU_L}{dL} = \frac{m^* \sigma_r{}^2 L}{E'}. \tag{50}$$

Combining these expressions and including, for comparison, the elastic energy released rate for a smooth path, one has for infinitesimal crack lengths,

$$G_0 = G_l \frac{dL_l}{dL_0}\left(\frac{m^*}{\pi}\right) = G\frac{dL}{dL_0} \tag{51}$$

Considering that the smooth crack length is equal to the projected crack length, one has

$$G_0 = G_l\left(\frac{m^*}{\pi}\right) = G\frac{dL}{dL_0} \tag{52}$$

Observe that the difference between the elastic energy released rate for the smooth, rugged and projected cracks is the ruggedness added on crack during its growth. Using a thermodynamic model for the crack propagation, it can be concluded that a rugged crack dissipates more energy than a smooth crack propagating at the same speed.

The elastic energy released rate G_0 can be written in terms of a fractal geometry,

$$G_0 = \frac{m^* \sigma_r^{\,2}}{E'} L_0 \left[1 + (2 - H) \left(\frac{H_0}{l_0} \right)^2 \left(\frac{l_0}{L_0} \right)^{2H-2} \right] \tag{53}$$

5.4. The crack growth resistance R for smooth, projected and rough paths

Considering a plane strain condition, crack growth resistance for a smooth crack is given by

$$R_l = \frac{dU_{\gamma l}}{dL_l} \tag{54}$$

Substituting equation (24) in equation (54), one finds

$$R_l = 2\gamma_l \tag{55}$$

Observe that if the fracture path is smooth, the specific surface energy γ_l is a cleavage surface energy and does not necessarily depend on the crack length. This model is only valid for brittle crystalline materials where the plastic strain at the crack tip does not absorb sufficient energy to cause dependence between fracture toughness and crack length.

Similarly, for a rugged crack, the fracture resistance to propagation is given by

$$R = 2\gamma_r \tag{56}$$

The concept of fracture growth resistance for the projected surface is given by

$$R_0 = \frac{dU_\gamma}{dL_0} \tag{57}$$

and substituting equation (26) in equation (57), one has

$$R_0 = 2\gamma_0 \tag{58}$$

Again, this model is valid for ideally brittle materials where there is almost no plastic strain at the crack tip. It basically corresponds to the model presented by Griffith, with a modified interpretation introduced by Irwin with the $G - R$ curve concept.

5.5. Relationship between rugged R and projected R_0 fracture resistances

Using the chain rule, and admitting Irwin´s energetic equivalence represented by equation (3), the projected fracture resistance can be written on the basis of the resistance of the real surface,

$$R_0 = R\frac{dL}{dL_0} \tag{59}$$

where dL/dL_0 is derived from equation (13),

$$\frac{dL}{dL_0} = \frac{1+(2-H)\left(\frac{H_0}{l_0}\right)^2\left(\frac{l_0}{L_0}\right)^{2H-2}}{\sqrt{2\left(1+\left(\frac{H_0}{l_0}\right)^2\left(\frac{l_0}{L_0}\right)^{2H-2}\right)}} \geq 1 \tag{60}$$

Therefore, the crack growth resistance (R-curve), which is defined for a flat projected surface, is given substituting equation (56) and equation (60) in equation (59),

$$R_0 = 2\gamma_r \frac{1+(2-H)\left(\frac{H_0}{l_0}\right)^2\left(\frac{l_0}{L_0}\right)^{2H-2}}{\sqrt{2\left(1+\left(\frac{H_0}{l_0}\right)^2\left(\frac{l_0}{L_0}\right)^{2H-2}\right)}} \tag{61}$$

5.6. Final remarks about equivalent quantities of smooth, rugged and projected fracture surfaces

It is important to emphasize that the energetic equivalence between the rugged surface crack path and its projection was considered such that the developed equations of the Fracture Mechanics for the flat plane path are still valid in the absence of any roughness.

However, if a flat and smooth fracture L_l is considered with the same length of a projected fracture L_0, the energetic quantities and their derivatives have the following relationship,

$$U_{Ll} \leq U_{L0} \rightarrow \frac{dU_L}{dL_l} \leq \frac{dU_{L0}}{dL_0} \rightarrow G_l \leq G_0 \tag{62}$$

and

$$U_{\gamma l} \leq U_{\gamma 0} \rightarrow \frac{dU_{\gamma l}}{dL_l} \leq \frac{dU_{\gamma 0}}{dL_0} \rightarrow R_l \leq R_{\gamma 0}, \tag{63}$$

which have produced conflicting conclusions in the literature [37, 38, 46]. Since the energy for the smooth length L_0^l is smaller than the energy for the projected L_0 or rough L lengths, one has

$$U_{Ll} \leq U_L \rightarrow G_l \leq G\frac{dL}{dL_0} \tag{64}$$

and

$$U_{\gamma l} \le U_{\gamma} \rightarrow R_{\gamma l} \le R\frac{dL}{dL_0} \tag{65}$$

In postulate III it was assumed that the rugged crack path satisfies the same energetic conditions of the plan path, but in the LEFM this roughness is not taken into account, causing discrepancies between theory and experiments. For example, it has not been possible to explain by an analytical function in a definitive way the growth of the $G-R$ curve. The proposed introduction of the term dL/dL_0 allows correcting this problem.

6. The elastic-plastic fractal fracture mechanics

The non-linear elastic plastic energy released rate J_0 for a crack of plane projected path can be extended from the Irwin-Orowan approach. They introduced the specific energy of plastic strain γ_p on the elastic energy released rate G_0 to describe the fracture phenomenon with considerable plastic strain at the crack tip. Thus, it is possible to define the elastic plastic energy released rate in an analogous way to the definition of the elastic energy released rate,

$$J_o \equiv \frac{d(F-U_{Vo})}{dL_o} \tag{66}$$

where U_{Vo} is the volumetric strain energy given by the sum of the elastic and plastic (U_{pl}) contributions to the strain energy in the material.

6.1. Influence of ruggedness in elastic plastic solids with low ductility

Considering elastic plastic materials with low ductility where the effect of the plastic term is small compared to the elastic term, one can define a crack growth resistance as

$$J_{Ro} = \frac{{K_{Ro}}^2 f(v)}{E}, \tag{67}$$

where $f(v)$ is a function that defines the testing condition. For plane stress $f(v)=1$, and for plane strain $f(v)=1-v^2$ and K_{Ro} is the fracture toughness resistance curve.

Due to the ruggedness, the crack grows an amount $dL > dL_0$ and correcting equation (59), one has

$$R_o = \frac{dU_{\gamma}}{dL}\frac{dL}{dL_o} = \left(2\gamma_e + \gamma_p\right)\frac{dL}{dL_o}. \tag{68}$$

Similarly,

$$J_o = \frac{d(F - U_V)}{dL}\frac{dL}{dL_o}. \tag{69}$$

The energy balance proposed by Griffith-Irwin-Orowan, for stable fracture, is

$$J_o = R_o. \tag{70}$$

Therefore, for plane stress or plane strain conditions, one can write from equation (61) that,

$$J_{Ro} = \left(2\gamma_e + \gamma_p\right)\frac{dL}{dL_o} = \frac{K_{Ro}{}^2 f(v)}{E} \tag{71}$$

Thus,

$$K_{Ro} = \sqrt{\frac{\left(2\gamma_e + \gamma_p\right)E}{f(v)}\frac{dL}{dL_o}}. \tag{72}$$

Knowing that fracture toughness is given by

$$K_{Co} = \sqrt{\frac{\left(2\gamma_e + \gamma_p\right)E}{f(v)}}, \tag{73}$$

one has,

$$K_{Ro} = K_{Co}\sqrt{\frac{dL}{dL_o}}. \tag{74}$$

From the Classical Fracture Mechanics, the fracture resistance for the loading mode I, is given by

$$K_{IRo} = Y_o\left(\frac{L_o}{w}\right)\sigma_f\sqrt{L_o}, \tag{75}$$

where $Y_o\left(\frac{L_o}{w}\right)$ is a function that defines the shape of the specimen (CT, SEBN, etc) and the type of test (traction, flexion, etc), and σ_f is the fracture stress. Considering the case when $L_0 = L_{0C}$, then $K_{IR0} = K_{IC0}$ and the fracture toughness for the loading mode I is given by

$$K_{ICo} = Y_o\left(\frac{L_{oc}}{w}\right)\sigma_f\sqrt{L_{oc}}. \tag{76}$$

Therefore, from equation (72) the fracture toughness curve for the loading mode I is given by

$$K_{IRo} = K_{ICo}\sqrt{\frac{dL}{dL_o}}. \tag{77}$$

Substituting equation (75) and equation (76) in equation (77), one has

$$\frac{dL}{dL_o} = Y_o^{\,2}\left(\frac{L_o}{w}\right)\frac{\sigma_f^{\,2}L_o f(v)}{\left(2\gamma_e+\gamma_p\right)E}, \tag{78}$$

Observe that according to the right hand side of equation (78), the ruggedness dL/dL_0 is determined by the condition of the test (plane strain or stress), the shape of the sample (CT, SEBN, etc), the type of test (traction, flexion, etc) and kind of material.

Considering the fracture surface as a fractal topology, one observes that the characteristics of the fracture surface listed above in equation (78) are all included in the ruggedness fractal exponent *H*. Substituting equation (60) in equation (71), one obtains

$$J_{Ro} = \left(2\gamma_e+\gamma_p\right)\frac{1+\left(2-H\right)\left(\frac{H_0}{l_0}\right)^2\left(\frac{l_0}{\Delta L_0}\right)^{2H-2}}{\sqrt{1+\left(\frac{H_0}{l_0}\right)^2\left(\frac{l_0}{\Delta L_0}\right)^{2H-2}}}. \tag{79}$$

which is non-linear in the crack extension ΔL_0 . It corresponds to the classical equation (70) corrected for a rugged surface with Hurst's exponent *H*. Experimental results [1, 2] show that J_0 and the crack resistance R_0 rise non-linearly and it is well known that this rising of the *J-R* curve is correlated to the ruggedness of the cracked surface [3, 4].

6.2. The J_0 Eshelby-Rice integral for rugged and plane projected crack paths

The *J*-integral concept of Eshelby-Rice is a non-linear extension of the definition given by Irwin-Orowan, for the linear elastic plastic energy released rate. In this context the potential energy Π_0 is defined as

$$\Pi_0 = \int_{V_0} W dV_0 - \int_C \vec{T}.\vec{u}ds, \tag{80}$$

where *W* the energy density integral in the in the volume V_0 encapsulated by the boundary C with tractions $\vec{T}$ and displacements $\vec{u}$, and *s* is the distance along the boundary C , as shown in Figure 4.

Accordingly,

$$J_0 = -\frac{d\Pi_0}{dL_0} = -\frac{d}{dL_0}\left(\int_V W dV_0 - \int_C \vec{T}.\vec{u}ds\right) \tag{81}$$

where dL_0 is the incremental growth of the crack length. In the two-dimensional case, where the fracture surface is characterized by a crack with length ΔL_0 and a unit thickness body, one has $dV = dxdy$ and

$$J_0 \equiv -\frac{d\Pi_0}{dL_0} = -\left(\int_V W \frac{dx}{dL_0} dy - \int_C \vec{T}.\frac{\partial \vec{u}}{\partial L_0} ds \right). \tag{82}$$

For a fixed boundary C, $d/dL_0 = -d/dx$, and the J_0 -integral for the plane projected crack path can be written only in terms of the boundary,

$$J_0 = \int_V W dy - \int_C \vec{T}.\frac{\partial \vec{u}}{\partial x} ds. \tag{83}$$

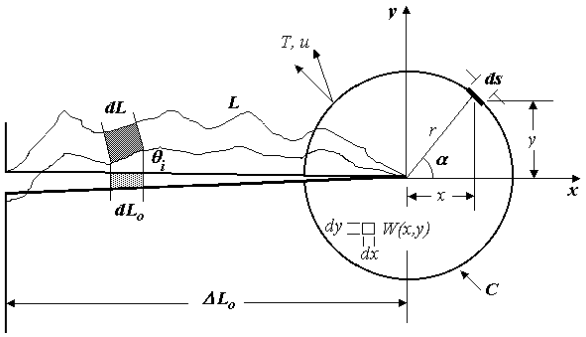

Figure 4. Boundary around to the rugged crack tip where is defined the *J*-Integral [43].

Now, the *J-R* Eshelby-Rice integral theory is modified to include the fracture surface ruggedness. Initially, equation (82) is rewritten,

$$J_0 = -\left(\int_V W \frac{dx}{dL} \frac{dL}{dL_0} dy - \int_C \vec{T}.\frac{\partial \vec{u}}{\partial L} \frac{dL}{dL_0} ds \right). \tag{84}$$

From postulate IV, the new *J*-integral on the rugged crack path is given by

$$J \equiv -\frac{d\Pi}{dL} = -\left(\int_V W \frac{dx^*}{dL} dy^* - \int_C \vec{T}.\frac{\partial \vec{u}}{\partial L} ds \right) \tag{85}$$

where the * symbol represents coordinates with respect to the rugged path. So, in an analogous way to the *J*-integral for the projected crack path given by equation (85), since $d/dL = -d/dx^*$, one has

$$J = \int_V W dy^* - \int_C \vec{T}.\frac{\partial \vec{u}}{\partial x^*} ds. \tag{86}$$

Returning to equation (82) and considering postulate III along with the derivative chain rule and substituting equation (85), one has

$$J_0 \equiv -\frac{d\Pi}{dL}\frac{dL}{dL_0} = -\left(\int_V W\frac{dx^*}{dL}dy^* - \int_C \vec{T}.\frac{\partial \vec{u}}{\partial L}ds\right)\frac{dL}{dL_0}. \tag{87}$$

Comparing (84) with equation (87) and considering that the rugged crack is a result of a transformation in the volume of the crack, analogous to the "*bakers´ transformation*" of the projected crack over the Euclidian plane, it can be concluded that

$$\begin{aligned} dx^*\,dy^* &= \frac{\partial(x^*,y^*)}{\partial(x,y)}dxdy \\ \frac{dx^*}{dL}dy^*\frac{dL}{dL_o} &= \frac{dx}{dL}\frac{dL}{dL_o}dy \end{aligned} \tag{88}$$

which show the equivalence between the volume elements,

$$dV = dx^*\,dy^* = dxdy. \tag{89}$$

Therefore, the ruggedness dL/dL_0 of the rugged crack path does not depend on the volume V, nor on the boundary C and nor on the infinitesimal element length ds or dy. Thus, it must depend only on the characteristics of the rugged path described by the crack on the material. Finally, the integral in equation (84) can be written as

$$J_0 = -\left(\int_V W\frac{dx}{dL}dy - \int_C \vec{T}.\frac{\partial \vec{u}}{\partial L}ds\right)\frac{dL}{dL_0} \tag{90}$$

where the infinitesimal increment $dx/dL = -\cos\theta_i$ accompanies the direction of the rugged path L, as show in Figure 4. Thus,

$$J = \int_V W dy\cos\theta_i - \int_C \vec{T}.\frac{\partial \vec{u}}{\partial x}\cos\theta_i ds. \tag{91}$$

Observe that the *J*-integral for the rugged crack path given by equation (91) differs from the *J*-integral for the plane projected crack path given by equation (83) by a fluctuating term, $\cos\theta_i$ inside the integral. It can be observed that the energetic and geometric parts of the fracture process are separated and put in evidence the influence of the ruggedness of the material in the elastic plastic energy released rate,

$$J_0 \equiv J\frac{dL}{dL_0}. \tag{92}$$

It must be pointed out that this relationship is general and the introduction of the fractal approach to describe the ruggedness is just a particular way of modeling.

6.3. Fractal theory applied to J-R curve model for ductile materials

This section includes the formalism of fractal geometry in the EPFM to describe the roughness effects on the fracture mechanical properties of materials. For this purpose the classical expression of the elastic-plastic energy released rate was modified by introducing the fractality (roughness) of the cracked surface. With this procedure the classical expression (49) of LEFM, linear with the crack length, is changed into a non-linear equation (53), which reproduces with precision the quasi-static crack propagation process in ductile materials.

Observe that the quasi-static crack growth condition is obtained with Griffith fracture criterion, doing $J_0 = R_0$ and $dJ_0 / dL_0 = dR_0 / dL_0$. In this case, it is concluded that the *J-R* curve is given by Griffith criterion $J = 2\gamma_{eff}$ in equations (92) and (59). Therefore, for a self-affine crack with $H_0 \to l_0$, one has

$$J_0 = 2\gamma_{eff} \frac{1 + (2 - H)\left(\frac{l_0}{L_0}\right)^{2H-2}}{\sqrt{2\left(1 + \left(\frac{H_0}{l_0}\right)^2 \left(\frac{l_0}{L_0}\right)^{2H-2}\right)}} \tag{93}$$

This model shows in unambiguous way how different morphologies (roughness) are correlated with the *J-R* curve growth. Given the energy equivalence between rough and projected surfaces for the crack path, the *J-R* curve increases due to the influence of the roughness, which has not been computed previously with the classical equations of EPFM.

The *J*-integral on the rugged crack path is a specific characteristic of the material and can be considered as being proportional to J_C [15], on the onset of crack extension, since in this case it has the rugged crack length greater than the projected crack length $(L \gg L_0)$. Thus,

$$J_o \sim J_C \frac{dL}{dL_o}. \tag{94}$$

Substituting the fractal crack model proposed in equation (60), one has

$$J_o \sim J_C \frac{1 + (2 - H)\left(\frac{H_0}{l_0}\right)^2 \left(\frac{l_o}{\Delta L_o}\right)^{2H-2}}{\sqrt{1 + \left(\frac{H_0}{l_0}\right)^2 \left(\frac{l_o}{\Delta L_o}\right)^{2H-2}}}, \tag{95}$$

corroborating that the surface specific energy is related to the critical fracture resistance.

$$J_C \sim \left(2\gamma_e + \gamma_p\right). \tag{96}$$

6.3.1. Case – 1. Ductile self-similar limit

The local self-similar limit can be calculated applying the condition $H_0 \to L_0 \gg l_0$ in equation (79), obtaining

$$J_{Ro} = \left(2\gamma_e + \gamma_p\right)(2-H)\left(\frac{l_o}{\Delta L_o}\right)^{H-1} \tag{97}$$

or, with $D = 2 - H$, one has

$$J_0 = 2\gamma_{eff} D\left(\frac{l_0}{L_0}\right)^{1-D}. \tag{98}$$

This result corresponds to the one found by Mu and Lung [26, 37] for ductile materials. Equation (98) is shown in Figure 5, where *J-R* curves are calculated for different values of the fractal dimension D. $2\gamma_{eff} = 10.0 KJ/m^2$ is adopted and L_0/l_0 is the crack length in l_0 units. This figure shows very clearly how the surface morphology (characterized by D) determines the shape of the *J-R* curve at the beginning of the crack growth.

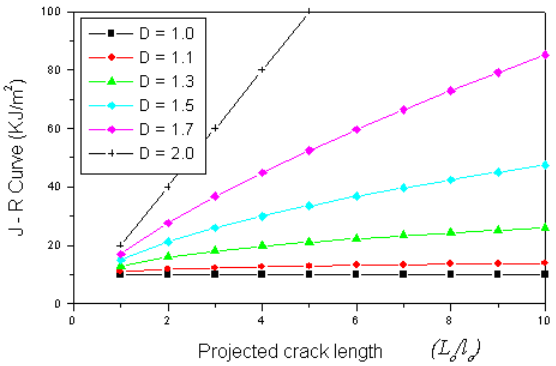

Figure 5. *J-R* curves calculated according to the projected crack length L_0, for a fracture of unit thickness, and fractal dimensions $D = 1.0, 1.1, 1.3, 1.5, 1.7$ and 2.0 with $2\gamma_e = 10 KJ/m^2$.

In Figure 6, *J-R* curves with fractal dimension $D = 1.3$ are calculated according to the projected length L_0 for different measuring rulers l_0, showing how the morphology of rugged surface cracks is best described for small values of l_0, causing the pronounced rising of *J-R* curve. Figure 6 and equation (98) show that the initial crack resistance is correlated to the surface morphology characterized by dimension D, in accordance with the literature.

The self-similar limit of *J-R* curve, given by equation (98), is valid only for regions near the onset of the crack growth in brittle materials ($H_0 \to L_0$). This is due to the hardening of the material, which gives rise to ruggedness of the fracture surface.

In the case of ductile materials, the length of the work hardening zone H_0 affects an increasingly greater area of the material as the crack propagates, but the self-similar limit $\left(H_0 = L_0 \gg l_0\right)$ is still valid.

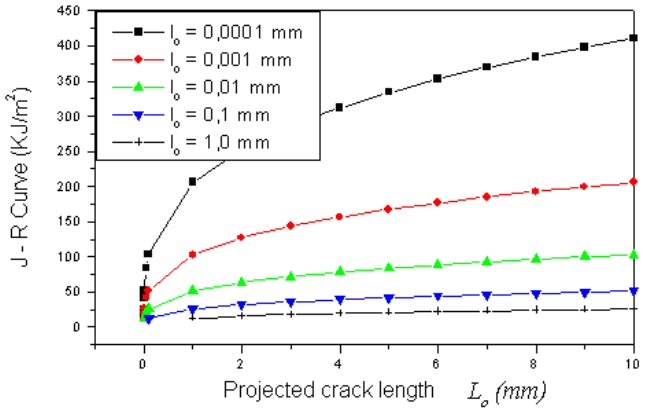

Figure 6. *J-R* curves calculated in function of the projected crack length L_0 with different ruler lengths $l_0 = 0.0001, 0.001, 0.01, 0.1$ and $1.0mm$, for a fracture of unit thickness, fractal dimension $D = 1.3$ and $2\gamma_e = 10KJ/m^2$.

However, in the case of brittle materials (ceramics), after the initial stage of hardening, the crack maintains this state in a region of length H_0, very short if compared to the crack length L_0, generating a self-similar fractal structure only when the crack length L_0 is small, in the order of l_0, i.e., $H_0 = L_0 = l_0$. When the crack length L_0 becomes much larger than the initial size of the hardening region H_0 present at the onset of crack growth, the self-similar limit is not valid, and the self-affine (or global) limit of fracture becomes valid.

6.3.2. Case – 2. Brittle self-affine limit

It is easy verify that in stable crack growth, where $J_0 = R_0$, using equations (59) and (79), one has $dL/dL_0 = 1$ when $L \to \infty$. The global self-affine limit of J_0 can be calculated applying the condition when the observation scale corresponds to a rather small amplitude of the crack, similar in size to the crack increment, i.e., when $H_0 \to l_0 \ll L_0$ in equation (79), resulting the linear elastic expression

$$J_0 = 2\gamma_{eff} \tag{99}$$

where $J_0 = G_0$ and

$$G_{Ro} = 2\gamma_e + \gamma_p. \tag{100}$$

This result corresponds to a classic one in Fracture Mechanics, which is the general case valid for brittle materials as glass and ceramics.

7. Experimental analyses

7.1. Ceramic, metallic and polyurethane samples

The analyzed ceramic samples were produced by Santos [19] and Mazzei [41]. The raw material used for its production was an alumina powder A-1000SG by ALCOA with 99% purity. Specimens of dimensions $52mm \times 8mm \times 4mm$ were sintered at 1650 °C for 2 hours, showing average 7 mm grain sizes. Their average mechanical properties are shown in Table 1 with elastic modulus E = 300 *GPa* and rupture stress $\sigma_f = 340MPa$.

The analyzed metallic samples were multipass High Strength Low Alloy (HSLA) steel weld metals and standard DCT specimens. HSLA are divided in two groups based on the welding process utilized and the microstructural composition. The first group (*A1* and *A2* welds) is composed of *C-Mn Ti-Killed* weld metals and were joined by a manual metal arc process. The second group (*B1* and *B2* welds), joined by a submerged arc welding process, is also a *C-Mn Ti-Killed* weld metal, but with different alloying elements added to increase the hardenability. Mechanical properties of both welds and DCT metals are listed in Table 1.

Material	*Sample*	σ_f *(MPa)*	*E (GPa)*	J_{IC}*(exp)(KJ/m²)*	L_{OC}*(exp)(mm)*	K_{IC} *(MPa.m$^{1/2}$)*	*H (exp)*
Ceramic	Alumina	340	300	0,030	0.4956	424,2477056	0,7975± 0,0096
Metals	A1CT2	516,00	1,34	291,60	0,48256	635,3313677	0,71 ± 0,01
	A2SEB2	537,00	3,63	174,67	0,36264	573,1747828	0,77 ± 0,01
	B1CT6	771,00	16,64	40,61	0,22634	650,1446157	0,77 ± 0,02
	B2CT2	757,00	1,96	99,22	0,26553	691,3971955	0,58 ± 0,05
	DCT1	554,00	1,7197	227,00	0,40487	624,8021278	-
	DCT2	530,00	1,6671	211,47	0,3995	593,7576222	-
	DCT3	198,75	0,3902	318,00	1,00000	352,2752029	-
Polymers	PU0,5	40,70	0.8 ± 0.0	8,10	0,29951	39,47980593	0,47 ± 0,07
	PU1,0	40,70	0.8 ± 0.0	3,00	0,23685	35,10799599	0,50 ± 0,05

Table 1. Data extracted from experimental testing of *J-R* curves obtained by compliance method.

The analyzed polymeric samples are a two-component Polyurethane, consisting of 1:1 mixture of polyol and prepolymer. The polyol was synthesized from oil and the prepolymer from diphenyl methane diisocyanate (MDI). Their mechanical properties are shown in Table 1.

7.2. Fracture tests

A standard three-point bending test was performed on alumina specimens, SE(B), notched plane. Low speed and constant prescribed displacement 1 *mm*/*min* was employed to obtain stable propagation. The *R*-curve was obtained using LEFM equations and fracture results are shown in Table 1.

The fracture toughness evaluation of metallic samples was executed using the *J*-integral concept and the elastic compliance technique with partial unloadings of 15% of the maximum load. For weld metals the *J-R* curve tests were performed by the compliance and multi-test techniques. Tests were executed in a MTS810 (Material Test System) system at ambient temperature, according to standard ASTM E1737-96 [15]. A single edge notch bending SENB and compact tension CT were used. One *J-R* curve for each tested specimen was retrieved and fracture results are shown in Table 1.

To obtain the fractured surfaces of polymeric materials, fracture toughness tests were performed by multiple specimen technique using the concept of *J-R* curve according to ASTM D6068-2002 [42]. However, these tests were different from the ones used for weld metals, due to the viscoelasticity of the polymers. The used nomenclatures PU0,5 and PU1,0 mean the loading rate used during the test, 0,5 *mm*/*min* and 1,0 *mm*/*min*, respectively. Fracture results are shown in Table 1.

7.3. Fractal analyses of fractured specimens

The fractured surfaces of ceramic samples were obtained with a Rank Taylor Hobson profilometer (Talysurf model 120) and an HP 6300 scanner. The fractal analyses to obtain the Hurst dimensions were made by methods, such as Counting Box, Sand Box and Fourier transform. The fracture surface analysis of metallic and polymeric samples were executed using scanning electronic microscopy SEM and the analyses to obtain the Hurst exponents were made with the Contrast Islands Fractal Analysis. Fractal dimension results are shown in the last column of Table 1.

7.4. G-R and J-R curve tests and fitting with self-similar and self-affine fractal models

A characteristic load-displacement result in the Alumina ceramic sample is shown in Figure 7. Observe that the stiffness of the material at the first deflection region is constant, corresponding to the elastic modulus of the material. However, as the crack propagates, the stiffness varies significantly.

The corresponding *G-R* curve test is shown in Figure 8. It can be seen that at the onset of crack growth ($L_0 \approx L_{0C}$), the behavior of this material is self-similar, as previously discussed. However, the results in the wider range of crack lengths ($L_{0C} < L_0 < L_{0\max}$) show that this material behave according to the self-affine model. Finally, at the end of *G-R* curve

($L_0 \to \infty$) the behavior is explained by the influence of the shape function $Y\left(L_0 / w\right)$ used in the testing methodology [41].

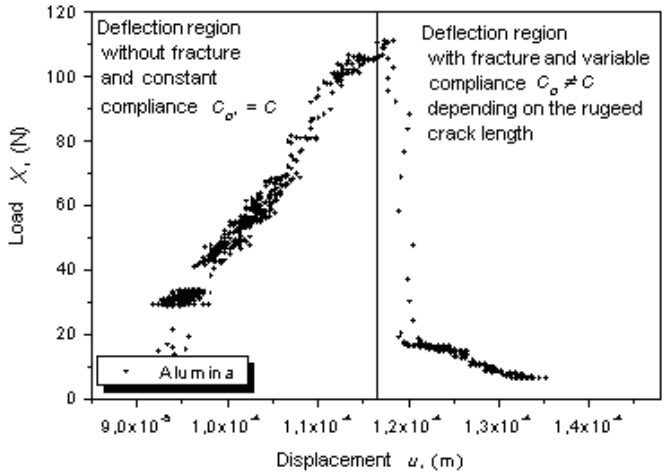

Figure 7. Load (X) versus displacement (u) for a *G-R* curve test in a ceramic sample [41].

J-R curves obtained from standard metallic specimens provided by ASTM standard testing are shown in Figure 9 along with the fitting with the proposed fractal models. Fitting results with these samples, named DCT1, DCT2 and DCT3, are a consistent validation of the applied fractal models. The fitting results of the self-similar and self-affine models coincide and are not distinguishable in Figure 9.

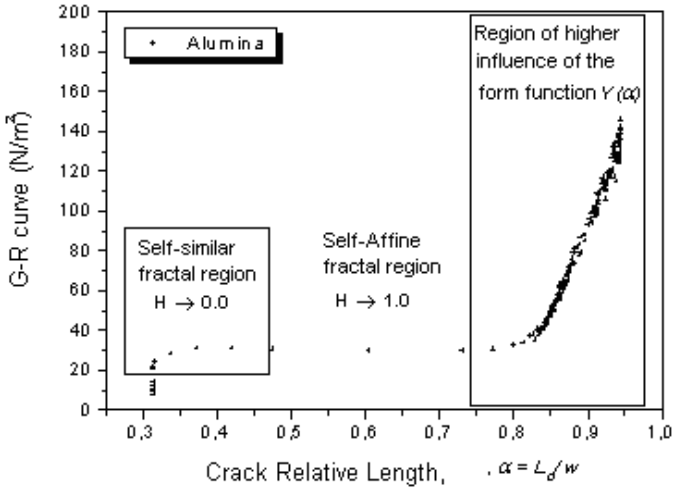

Figure 8. *G-R* curve fitted with the self-similar model (equation (97)) and the self-affine model (equation (100)) for the Alumina sample [41].

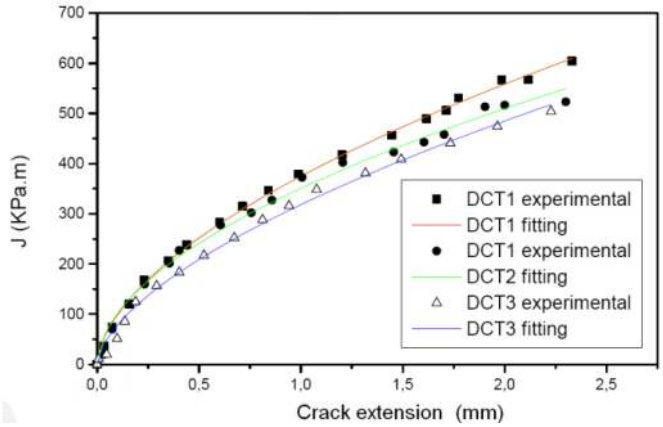

Figure 9. *J-R* curve fitted with the self-similar model shown in equation (97) and the self-affine model shown in equation (93) for steel samples DCT1, DCT2 and DCT3 [43].

Typical testing results performed to obtain *J-R* curves of metallic weld materials are shown in Figure 10 and Figure 11. In all results, *J-R* curves measured experimentally were fitted using models given by equations (93) and (97), where the factor $2\gamma_e + \gamma_p$ was obtained by adjusting the l_0 and H values for each different sample, by the self-similar and the self-affine models.

The *J-R* curves for the tested polymeric specimens are shown in Figure 12 and Figure 13. Reasonably good results were obtained despite the greater dispersion of data.

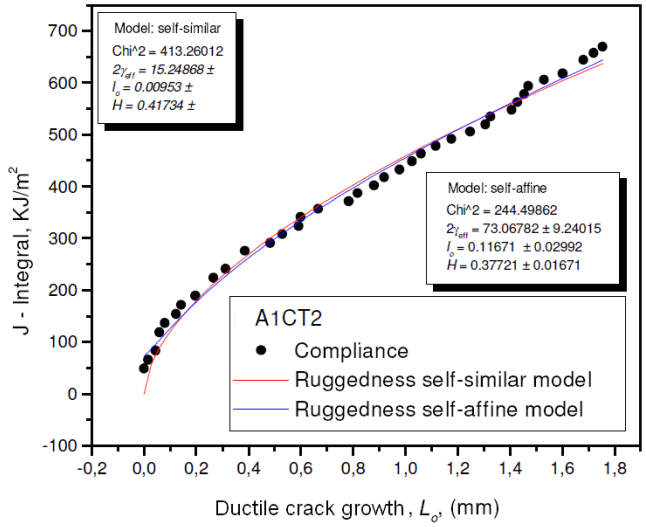

Figure 10. *J-R* curve fitted with the self-similar model shown in equation (97) and the self-affine model shown in equation (93) for HSLA-Mn/Ti steel (sample A1CT2).

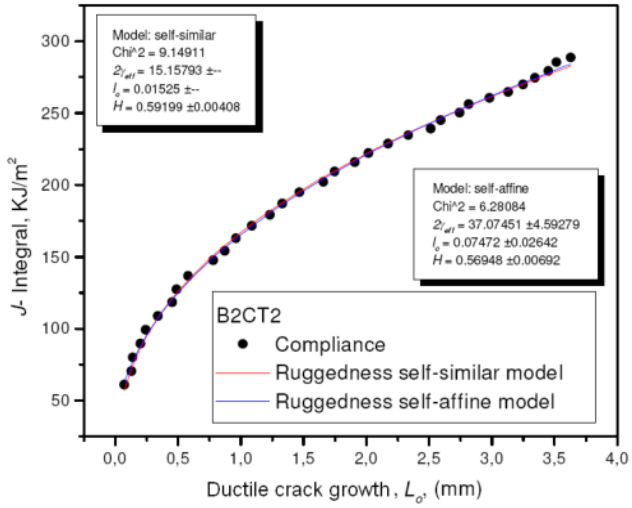

Figure 11. *J-R* curve fitted with the self-similar model shown in equation (97) and the self-affine model shown in equation (93) for HSLA-Mn/Ti steel (sample B2CT2) killed with titanium and other alloy elements to increase hardenability [43].

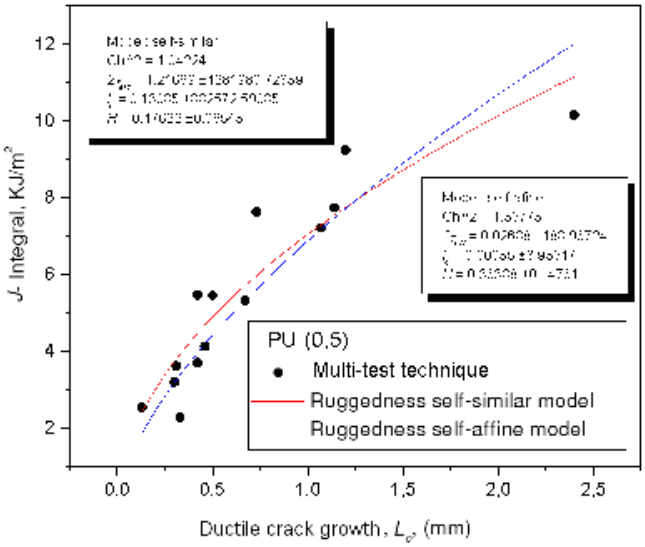

Figure 12. *J-R* curve fitted with the self-similar model shown in equation (97) and the self-affine model shown in equation (93) for the poliurethane polymer PU0,5.

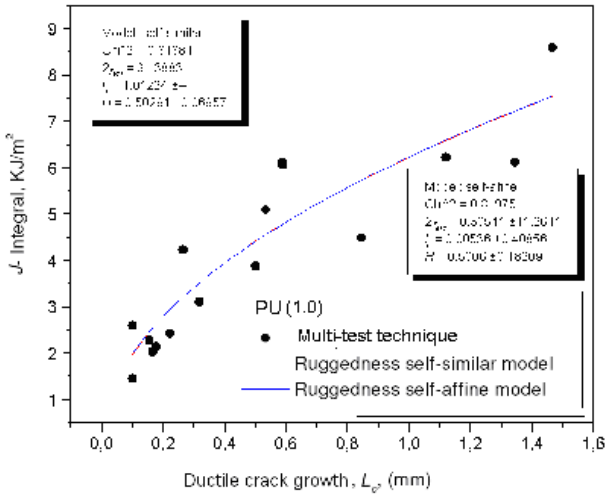

Figure 13. *J-R* curve fitted with the self-similar model shown in equation (97) and the self-affine model shown in equation (93) for the poliurethane polymer PU1,0.

After the experimental *J-R* curves were fitted using equation (79) and equation (97), values of $2\gamma_{eff}$, H and l_0 were determined and are shown in Table 2 and Table 3. With $J_{R0} = 2\gamma_{eff}$, the value of the crack size $L_{0\gamma_{eff}}$ was calculated and it corresponded to the specific surface energy. Using the experimental values of J_{IC}, L_{0C} and H given in Table 1, the values of the constants in the last column of Table 2 and Table 3 were calculated.

Material	*Sample*	$2\gamma_{eff}\left(KJ/m^2\right)$	$H(theo)$	$l_0(mm)$	$L_{0\gamma_{eff}} = l_0(2-H)^{1/(H-1)}$	$C_1/2\gamma_{eff} = (2-H)l_0^{H-1}$	$J_C L_C{}^{H-1} = constant$
Ceramic	Alumi-na	0,0301871	1,000	0,2493645	0,2493645	1,00000	0,03018707
Metals	A1CT2	283,247	0,417 ± 0,018	1,00944	0,459079	1,57411	445,862579
	A2SEB2	187,639	0,208 ± 0,057	0,82912	0,396956	2,07868	390,042318
	B1CT6	40,514	0,573 ± 0,038	0,51758	0,225086	1,89071	76,600193
	B2CT2	101,204	0,592 ± 0,0041	0,64484	0,278764	1,68407	170,433782
	DCT1	230,843	0,426	0,91887	0,416893	1,65219	381,397057
	DCT2	209,127	0,461	0,87082	0,391328	1,65806	346,745868
	DCT3	317,819	0,393	2,18249	0,999062	1,00057	318,000000
Poly-mers	PU0,5	17,4129	0,476	2,88612	1,291434	0,87464	15,230001
	PU1,0	2,95252	0,503	0,51653	0,229374	2,079	6,138287

Table 2. Fitting data of *J-R* curves with the self- similar model [43].

A good level of agreement is seen between measured Hurst's exponents H at Table 1 and theoretical ones shown in Table 2 and Table 3. Larger differences in metals can be attributed to the quality of the fractographic images, which did not present well defined "Contrast Islands".

Material	Sample	$2\gamma_{eff}\left(KJ/m^2\right)$	$H(theo)$	$l_0(mm)$	$L_{0\gamma_{eff}} = l_0\left(2-H\right)^{1/(H-1)}$	$C_1/2\gamma_{eff} = \left(2-H\right)l_0^{H-1}$	$J_C {L_C}^{H-1} = constant$
Ceramic	Alumina	0,0301871	1,000	0,2493645	0,2493645	1,00000	0,03018707
Metals	A1CT2	160,640	0,609	0,24422	0,105004	2,413408	387,700806
	A2SEB2	102,750	0,442	0,31002	0,140040	2,993092	307,535922
	B1CT6	22,980	0,700	0,08123	0,033873	2,757772	63,385976
	B2CT2	57,978	0,705	0,10304	0,042893	2,529433	146,651006
	DCT1	129,850	0,599	0,23309	0,100540	2,511844	326,184445
	DCT2	118,850	0,624	0,20167	0,086294	2,512302	298,592197
	DCT3	178,810	0,612	0,5282	0,226901	1,778386	318,000000
Polymers	PU0,5	7,500	0,664	0,56541	0,238775	1,618852	12,150370
	PU1,0	1,690	0,649	0,10898	0,046244	2,938220	4,971102

Table 3. Fitting data of *J-R* curves with the self- affine model [43].

7.5. Complementary discussion

The proposed fractal scaling law (self-affine or self-similar) model is well suited for the elastic-plastic experimental results. However, the self-similar model in brittle materials appears to underestimate the values of specific surface energy γ_{eff} and the minimum size of the microscopic fracture l_0, although not affecting the value of the Hurst exponent H.

For a self-affine natural fractal such as a crack, the self-similar limit approach is only valid at the beginning of the crack growth process [39], and the self-affine limit is valid for the rest of the process. It can be observed from the results that the ductile fracture is closer to self-similarity while the brittle fracture is closer to self-affinity.

Equation (79) represents a self-affine fractal model and demonstrates that apart from the coefficient H, there is a certain "universality" or, more accurately, a certain "generality" in the *J-R* curves. This equation can be rewritten using a factor of universal scale, $\varepsilon = l_0 / L_0$, as

$$\underbrace{f(2\gamma_e+\gamma_p, J_0) = \frac{J_o}{2(2\gamma_e+\gamma_p)}}_{energetic} = \underbrace{\frac{1+(2-H)\varepsilon^{2H-2}}{\sqrt{2\left(1+\varepsilon^{2H-2}\right)}} = g(\varepsilon, H)}_{geometric} \tag{101}$$

which is a valid function for all experimental results shown in Figure 14. It shows the existent relation between the energetic and geometric components of the fracture resistance

of the material. The greater the material energy consumption in the fracture, straining it plastically, the longer will be its geometric path and more rugged will be the crack.

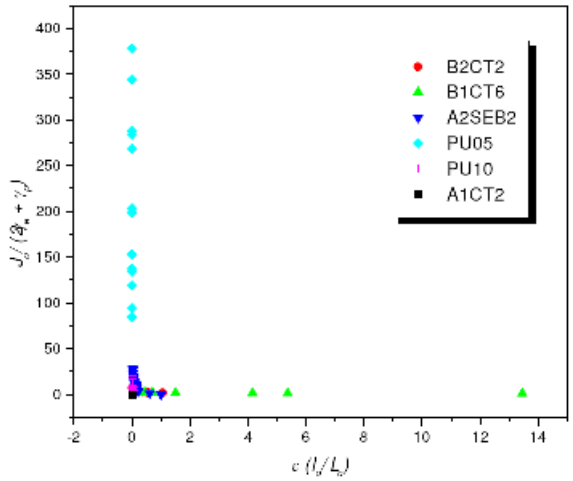

Figure 14. Generalized *J-R* curves for different materials, modelled using the self-affine fractal geometry, in function of the scale factor $\varepsilon = l_0/L_0$ of the crack length [43].

In the self-similar limit $(l_0 \ll L_0 = H_0)$, equation (97) is applicable and the energetic and geometric components are put in evidence in the equation below,

$$J_0 = \underbrace{(2\gamma_{eo} + \gamma_p)}_{energetic} \underbrace{(2-H)\left(\frac{l_0}{\Delta L_0}\right)^{H-1}}_{geometric} \tag{102}$$

From equation (102), an expression can be derived which results in a constant value associated to each material,

$$\underbrace{J_0 \Delta L_0}_{macroscopic}{}^{H-1} = \underbrace{(2\gamma_{e0} + \gamma_p)(2-H) l_0{}^{H-1}}_{microscopic} = (const)_{material} \tag{103}$$

It is possible to conclude that the macroscopic and microscopic terms on the left and right-hand sides of equation (103) are both equal to a constant, suggesting the existence of a fracture fractal property valid for the beginning of crack growth, and justified experimentally and theoretically. These constant values were calculated for each point in each *J-R* curve for the tested materials. The average value for each material is listed in the last column of Table 2 and Table 3. Observe that this new property is uniquely determined by the process of crack growth, depending on the exponent H, the specific surface energy $2\gamma_e + \gamma_p$ and the minimum crack length l_0.

This new constant can be understood as a "fractal energy density" and it is a physical quantity that takes into account the ruggedness of the fracture surface and other physical properties. Its existence can explain the reason for different problems encountered when defining the value of fracture toughness K_{IC}. This constant can be used to complement the information yielded by the fracture toughness, which depends on several factors, such as the thickness B of the specimen, the shape or size of the notch, etc. To solve this problem, ASTM E1737-96 [15] establishes a value for the crack length a (approximately $0.5 < a/W < 0.7$ and, $B = 0.5W$, where W is the width of the specimen) for obtaining the fracture toughness K_{IC}, in order to maintain the small-scale yielding zone.

As shown in equation (103), a relationship exists between the specific surface energy $2\gamma_{eff}$ and the minimum crack size l_0 in the considered observation scale $\varepsilon = l_0 / L_0$. In Figure 15, it can be observed that the consideration of a minimum size for the fracture l_{01} on a grain should mean the effective specific energy of the fracture $2\gamma_{eff1}$ in this scale. In a similar way, the consideration of a minimum size of fracture in a different scale, like one that involves several polycrystalline grains l_{02}, l_{03} etc.., should take into account the value of an effective specific energy in this other scale, $2\gamma_{eff2}, 2\gamma_{eff3}$, etc., in such a way that

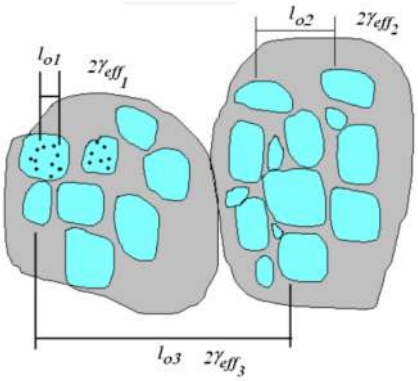

Figure 15. Microstructural aspects of the observation scale with different l_0 ruler sizes, for the fractal scaling of fracture [43].

$$2\gamma_{ef1}(2-H_1)l_{o1}{}^{H_1-1} = 2\gamma_{eff2}(2-H_2)l_{o2}{}^{H_2-1} = const, \tag{104}$$

although $l_{01} \neq l_{02} \neq l_{03}$ and $2\gamma_{eff1} \neq 2\gamma_{eff2} \neq 2\gamma_{eff3}$. So, the constant does not depend on the single rule of measurement l_0 used in the fractal model, but it depends on the kind of material used in the testing.

Another interpretation of equation (102) can be made by splitting the elastic and plastic terms,

$$J_0 = \underbrace{2\gamma_e(2-H)\left(\frac{l_0}{\Delta L_0}\right)^{H-1}}_{elastic} + \underbrace{\gamma_p(2-H)\left(\frac{l_0}{\Delta L_0}\right)^{H-1}}_{plastic}, \tag{105}$$

For the particular situation where $J_0 = J_{IC}$ and $\Delta L_0 = \Delta L_{0C}$, it can be derived from equation (97),

$$J_{IC} = \left(2\gamma_e + \gamma_p\right)\left(2-H\right)\left(\frac{l_0}{L_{0C}}\right)^{H-1} \tag{106}$$

and from equation (72),

$$K_{IC} = \sqrt{(2\gamma_e + \gamma_p)E(2-H)\left(\frac{l_o}{L_{oc}}\right)^{H-1}} \tag{107}$$

Therefore, using the fact that once the experimental value of J_{IC} is determined and the fitting of *J-R* curve has already yielded the values $2\gamma_e + \gamma_p, l_0$ and H for the material, the value L_{0C} can be calculated.

Fracture Mechanics science was originally developed for the study of isotropic situations and homogeneous bodies.

At the microscopic level, the elastic material is modeled considering Einstein's solid harmonic approximation where Hooke's law is employed for the force between the chemical bonds of the atoms or molecules [48]. Therefore, the elastic theory is used to make linear approximations and it does not involve micro structural effects of the material.

At the mesoscopic level the equation of energy used for the fracture does not take into account effects at the atomic scale involving non-homogeneous situations [47]. Based on the arguments of the last paragraphs, it becomes clear why Herrmman *et al*. [49] needed to include statistical weights, as a crack growth criterion, for the break of chemical bonds in fracture simulations, as a form of portraying micro structural aspects of the fracture (defects) when using finite difference and finite element methods in computational models.

At the macroscopic level, on the other hand, Griffith's theory uses a thermodynamic energy balance. It is important to remember that the linear elastic theory of fracture developed by Irwin and Westergaard and the Griffith's theory are differential theories for the macroscopic scale, which means they are punctual in their local limit. These two approaches involve the micro structural aspects of the fracture, since they take a larger infinitesimal local limit than the linear elastic theory at the atomic and mesoscopic scales. This infinitesimal macroscopic scale is big enough to include 10^{15} particles as the lower thermodynamic limit, where the physical quantity Fracture Resistance (*J-R* Curve) portrays aspects of the interaction of the crack with the microstructure of the material.

In this chapter, Classical Fracture Mechanics was modified directly using fractal theory, without taking into account more basic formulations, such as the interaction force among particles, or Lamé's energy equation in the mesoscopic scale as a form to include the ruggedness in the fracture processes.

The use of the fractality in the fracture surface to quantify the physical process of energy dissipation was approached with two different proposals. The first was given by Mu and Lung [26, 37], who proposed a phenomenological exponential relation between crack length and the elastic energy released rate in the following form

$$G_{IC} = G_{I0}\varepsilon^{1-D}, \tag{108}$$

where ε is the length of the measurement rule. The second proposal was given by Mecholsky *et al*. [24] and Mandelbrot *et al*. [23], who suggested an empirical relation between the fractional part of the fractal dimension D^* and fracture toughness K_{IC},

$$K_{IC} \sim A\left(D^*\right)^{1/2} \tag{109}$$

where $A = E_0\sqrt{l_0}$ is a constant and E_0 is the stiffness modulus and l_0 is a parameter that has a unit length (an atomic characteristic length). The elastic energy released rate is then given by,

$$G_0 = El_0D^* \tag{110}$$

where $G_{0C} = K_{IC}^2 / E$ is the critical energy released rate.

The authors cited above used the Slit Island Method in their measurements of the fractal dimension D and it is important to emphasize that both proposals have plausible arguments, in spite of their mathematical differences. Observe that in the proposal of Mu and Lung [26, 37] the fractal dimension appears in the exponent of the scale factor, while in the proposal of Mecholsky *et al*. [24] and Mandelbrot *et al*. [23] the fractal dimension appears as a multiplying term of the scale factor.

The mathematical expression proposed in this work, equation (93) and equation (97), for the case $J_0 \equiv G_0$, is compatible with the two proposals above and can be seen as a unification of these two different approaches in a single mathematical expression. In other words, the two previous proposals are complementary views of the problem according to the expression deduced in this chapter.

A careful experimental interpretation must be done from results obtained in a *J-R* curve test. The authors mentioned above worked with the concept of G, valid for brittle materials, and not with the concept of J valid for ductile materials. The experimental results show that for the case of metallic materials the fitting with their expressions are only valid in the initial development of the crack because of the self-similar limit, while self-affinity is a general characteristic of the whole fracture process [39].

The plane strain is a mathematical condition that allows defining a physical quantity called K_{IC}, which doesn't depend on the thickness of the material. The measure of an average crack size along the thickness of the material, according to ASTM E1737-96 [15], is taken as an average of the crack size at a certain number of profiles along the thickness. In this way, any self-affine profile, among all the possible profiles that can be obtained in a fracture surface, are statistically equivalent to each other, and give a representative average for the Hurst exponent.

The crack height (corresponding to the opening crack test CTOD) follows a power law with the scales, $\varepsilon_h = \varepsilon_v = \varepsilon = l_0 / \Delta L_0$ and can be written as,

$$\frac{\Delta H_0}{h_0} = \left(\frac{\Delta L_0}{l_0} \right)^{1-H} \tag{111}$$

This relation shows that, while the measurement of the number of units of the crack length $N_h = \Delta L_0 / l_0$ in the growth direction grows linearly, the number of units of the crack height units $N_v = \Delta H_0 / l_0$ grows with a power of $1 - H$. If it is considered that the inverse of the number of crack increments in the growth direction $N_h^{-1} = l_0 / \Delta L_0$ is also a measure of strain of the material, as the crack grows, and considering that the number of crack height increments can be a measure of the amount of the piling up dislocation, in agreement with equation (111), then the normal stress is of the type [44, 45]

$$\sigma \sim \varepsilon^{-H} \tag{112}$$

Observe that this relation shows a homogeneity in the scale of deformations, similar to the power law hardening equation [34]. This shows that the fractal scaling of a rugged fracture surface is related to the power law of the hardening. It is possible that the fractality of the rugged fracture surface is a result of the accumulation of the pilled up dislocations in the hardening of the material before the crack growth.

In all three situations (metallic, polymer and ceramic) the presence of microvoids, or other microstructural defects, cooperate with the formation of ruggedness on the fracture surface. This ruggedness on the way it was modeled records the "history" of crack growth being responsible for the difficulty encountered by the crack to propagate, thus defining the crack growth resistance. In EPFM literature, the rising of *J-R* curve for a long time has been associated with the interposition of plane stress and plane strain conditions generating the unique morphology of the fracture surface ruggedness [1, 2]. In metals this rising has been associated with the growth and coalescence of microvoids [2]. However, the Fractal EPFM has proposed that the morphology of the fracture surface, characterized by parameters of fractal geometry, explains in a simple and direct way the rising of the *J-R* curves.

The success of fracture fractal modeling between the *J-R* curve and the exponent H can be attributed to the following fact: a fracture occurs only after a process of hardening in the

material, even minimal. Such a process follows a power law [35], self-similar [33], of the stress applied, σ with the strain ε, as shown in equation (166). It is therefore possible to associate the *elasto-plastic energy released rate* J which is an energetic quantity with the applied stress σ, which is an *energy density*, and the *fracture length* L_0 with strain, and $\varepsilon = \Delta l / l$ and the ruggedness exponent H with the strain hardening exponent "n" [15]. As the strain hardening occurs before the onset of crack growth, it is evident that its physical result appears registered in the fracture surface in terms of ruggedness, created in the process of crack growth. This process of crack growth admits a fractal scaling in terms of the projected surface L_0, so it is possible that the effect of its prior work hardening is responsible for the further self-affinity of fracture valid at the beginning of crack growth. This is because in the limit of the beginning of crack growth, the fractal scaling relationship is a self-similar power law, analogous to the power law hardening relationship [8, 33].

The technical standards ASTM E813 [40] and ASTM E1737-96 [15] suggest an exponential fitting of the type

$$J_0 = C_1 \Delta {L_0}^{C_2} \tag{113}$$

for the *J-R* curves. They do not supply any explanation for the nature of the coefficients for this fitting. However, by comparing equation (113) with equation (97), it can be concluded that $C_1 = 2\gamma_{eff}\left(2-H\right)l_0^{H-1}$ and $C_2 = 1-H$, which explains the physical nature of this parameters;

8. Conclusions

The theory presented in this chapter introduces fractal geometry (to describe ruggedness) in the formalism of classical EPFM. The resulting model is consistent with the experimental results, showing that fractal geometry has much to contribute to the advance of this particular science.

It was shown that the rising of the *J-R* curve is due to the non-linearity in Griffith-Irwin-Orowan's energy balance when ruggedness is taken into account. The idea of connecting the morphology of a fracture with physical properties of the materials has been done by several authors and this connection is shown in this chapter with mathematical rigor.

It is important to emphasize that the model proposed in this chapter illuminates the nature of the coefficients for the fitting proposed by the fractal model, which is the true influence of ruggedness in the rising of the *J-R* curve. The application of this model in the practice of fracture testing can be used in future, since the techniques for obtaining the experimental parameters, l_0, H, and γ_{eff} can be accomplished with the necessary accuracy.

The method for obtaining the *J-R* curves proposed in this chapter does not intend to substitute the current experimental method used in Fracture Mechanics, as presented by the ASTM standards. However, it can give a greater margin of confidence in experimental

results, and also when working with the microstructure of the materials. For instance, in search of new materials with higher fracture toughness, once the model explains micro and macroscopically the behavior of *J-R* curves.

It is well known that the fracture surfaces in general are multifractal objects [9] and the treatment presented here applies only to monofractals surfaces. However, for purposes of demonstrating the ruggedness influence on the phenomenology of Fracture Mechanics, through the models presented in this chapter, the obtained results were satisfactory. The generalization by multifractality is a matter to be discussed in future work.

Author details

Lucas Máximo Alves
GTEME – Grupo de Termodinâmica, Mecânica e Eletrônica dos Materiais,
Departamento de Engenharia de Materiais, Universidade Estadual de Ponta Grossa, Uvaranas,
Ponta Grossa – PR, Brazil

Luiz Alkimin de Lacerda
LACTEC – Instituto de Tecnologia para o Desenvolvimento, Departamento de Estruturas Civis,
Centro Politécnico da Universidade Federal do Paraná, Curitiba – PR, Brazil

9. References

[1] Kraff, J.M.; Sullivan, A.M.; Boyle, R.W. (1962) Effect of Dimensions on Fast Fracture Instability of Notched Sheets. In: Proceedings of the Cracks Propagation Symposium Cranfield. England: The College of Aeronautics, Cranfield. 1: pp.8-28.

[2] Ewalds, H.L.; Wanhill, R.J.H. (1986) Fracture Mechanics. Netherlands: Delftse Uitgevers Maatschappij, Third Edition, Co-Publication of Edward Arnold Publishers, London 1993.

[3] Hübner, H.; Jillek, W. (1977) Subcritical Crack Extension and Crack Resistance In Polycrystaline Alumina. J. Mater. Sci. 12(1): 117-125.

[4] Swanson, P.L.; Fairbanks, C.J.; Lawn, B.R.; Mai, Y-M.; Hockey, B.J. (1987) Crack-Interface Grain Bridging as a Fracture Resistance Mechanism In Ceramics: I, Experimental Study on Alumina, J. Am. Ceram. Soc. 70(4): 279-289.

[5] Mandelbrot, B.B. (1982) The Fractal Geometry of Nature, San Francisco, Cal-USA, New York: W. H. Freeman and Company.

[6] Underwood, E.E.; Banerji, K. (1992) Quantitative Fractography,. Engineering Aspectes of Failure and Failure Analysis. In: ASM - Handbook Fractography - The Materials Information Society. ASTM 1996. 12: pp. 192-209

[7] Dauskardt, R. H.; Haubensak, F.; Ritchie, R.O. (1990) On the Interpretation of the Fractal Character of Fracture Surfaces; Acta Metall. Matter. 38(2): 143-159.

[8] Borodich, F. M. (1997) Some Fractal Models of Fracture. J. Mech. Phys. Solids. 45(2): 239-259.

[9] Xie, H.; Wang, J-A.; Stein, E. (1998) Direct Fractal Measurement and Multifractal Properties of Fracture Surfaces, Physics Letters A. 242: 41-50.
[10] Herrmann, H.J.; Stéphane, R. (1990) Statistical Models For the Fracture of Disordered Media, Random Materials and Processes. In: Series Editors: H. Eugene Stanley and Etienne Guyon editors. Amsterdam: North-Holland.
[11] Rodrigues, J.A.; Pandolfelli, V.C (1998) Insights on the Fractal-Fracture Behaviour Relationship. Materials Research. 1(1): 47-52.
[12] Mecholsky, J. J.; Passoja, D.E.; Feinberg-Ringel, K.S. (1989) Quantitative Analysis of Brittle Fracture Surfaces Using Fractal Geometry, J. Am. Ceram. Soc. 72(1): 60-65.
[13] Tanaka, M. (1996) Fracture Toughness and Crack Morphology in Indentation Fracture of Brittle Materials. Journal of Materials Science. 31: 749-755.
[14] Xie, H. (1989) The Fractal Effect of Irregularity of Crack Branching on the Fracture Toughness of Brittle Materials. International Journal of Fracture. 41: 267-274.
[15] ASTM E1737 (1996) Standard Test Method For J-Integral Characterization of Fracture Toughness. pp.1-24.
[16] Alves, L.M. (2005) Fractal Geometry Concerned with Stable and Dynamic Fracture Mechanics. Journal of Theoretical and Applied Fracture Mechanics. 44(1): 44-57.
[17] Williford, R. E. (1990) Fractal Fatigue. Scripta Metallurgica et Materialia. 24: 455-460.
[18] Chelidze, T.; Gueguen, Y. (1990) Evidence of Fractal Fracture, (Technical Note) Int. J. Rock. Mech Min. Sci & Geomech Abstr. 27(3): 223-225.
[19] Dos Santos, S.F. (1999) Aplicação do Conceito de Fractais para Análise do Processo de Fratura de Materiais Cerâmicos, Dissertação de Mestrado, Universidade Federal de São Carlos, São Carlos.
[20] Alves, L.M.; Silva, R.V.; Mokross, B.J. (2001) The Influence of the Crack Fractal Geometry on the Elastic Plastic Fracture Mechanics. Physica A: Statistical Mechanics and Its Applications. 295(1/2): 144-148.
[21] Mandelbrot, B.B. (1977) Fractals: Form Chance and Dimension, San Francisco, Cal-USA: W. H. Freeman and Company.
[22] Passoja, D.E.; Amborski, D.J. (1978) In Microsstruct. Sci. 6: 143-148.
[23] Mandelbrot, B.B.; Passoja, D.E.; Paullay, A.J. (1984) Fractal Character of Fracture Surfaces of Metals, Nature (London), 308 [5961]: 721-722.
[24] Mecholsky, J.J.; Mackin, T.J.; Passoja, D.E. (1988) Self-Similar Crack Propagation In Brittle Materials. In: Advances In Ceramics, Fractography of Glasses and Ceramics, the American Ceramic Society, Inc. J. Varner and V. D. Frechette editors. Westerville, Oh: America Ceramic Society 22: pp. 127-134.
[25] Rodrigues, J.A.; Pandolfelli, V.C. (1996) Dimensão Fractal e Energia Total de Fratura. Cerâmica 42(275).
[26] Mu, Z.Q.; Lung, C.W. (1988) Studies on the Fractal Dimension and Fracture Toughness of Steel, J. Phys. D: Appl. Phys. 21: 848-850.
[27] Gong, B.; Lai, Z.H. (1993) Fractal Characteristics of *J-R* Resistance Curves of Ti-6Al-4V Alloys, Eng. Fract. Mech. 44(6): 991-995.
[28] Yavari, A. (2002) The Mechanics of Self-Similar and Self-Afine Fractal Cracks, Int. Journal of Fracture. 114: 1-27.

[29] Borodich, F. M. (1994) Fracture energy of brittle and quasi-brittle fractal cracks. Fractals in the Natural and Applied Sciences(A-41), Elsevier, North-Holland, 61–68.
[30] Carpinteri, A.; Chiaia, B. (1996) Crack-Resistance as a Consequence of Self-Similar Fracture Topologies, International Journal of Fracture, 76: 327-340.
[31] Bouchaud, E.; Bouchaud, J.P. (1994) Fracture Surfaces: Apparent Roughness, Relevant Length Scales, and Fracture Toughness. Physical Review B, 50(23): 17752–17755.
[32] Mosolov, A.B.; Borodich, F.M. (1992) Fractal Fracture of Brittle Bodies During Compression, Sovol. Phys. Dokl., May. 37(5): 263-265.
[33] Mosolov, A.B. (1993) Mechanics of Fractal Cracks In Brittle Solids, Europhysics Letters, 10 December. 24(8): 673-678.
[34] Anderson, T.L. (1995) Fracture Mechanics, Fundamentals and Applications. CRC Press, 2th Edition.
[35] Kanninen, M.F.; Popelar, C.H. (1985) Advanced Fracture Mechanics, the Oxford Engineering Science Series 15, Editors: A. Acrivos, et al. Oxford: Oxford University Press. Chapter 7, p. 437.
[36] Cherepanov, G.P.; Balankin, A.S.; Ivanova, V.S. (1995) Fractal fracture mechanics–A review. Engineering Fracture Mechanics, 51(6): 997-1033.
[37] Lung, C.W.; Mu, Z.Q. (1988) Fractal Dimension Measured with Perimeter Area Relation and Toughness of Materials, Physical Review B, 38(16): 11781-11784.
[38] Lei, W.; Chen, B. (1995) Fractal Characterization of Some Fracture Phenomena, Eng. Fract. Mechanics. 50(2): 149-155.
[39] Mandelbrot, B.B. (1991) Self-affine Fractals and Fractal Dimension. In: Family, Fereydoon. and Vicsék, Tamás editors. Dynamics of Fractal Surfaces. Singapore: World Scientific. pp.19-39.
[40] ASTM E813, (1989) Standard Test Method For J_{ic}, A Measure of Fracture Toughness.
[41] Mazzei, A.C.A. (1999) Estudo sobre a determinação de curva-R de compósitos cerâmica-cerâmica. Tese de Doutorado, DEMA-UFScar.
[42] ASTM D6068 - 10 (2002) Standard Test Method for Determining *J-R* Curves of Plastic Materials, crack growth resistance, fracture toughness, JR curves, plastics, 96.
[43] Alves, L.M.; Da Silva, R.V.; De Lacerda, L.A. (2010) Fractal Modeling of the *J-R* Curve and the Influence of the Rugged Crack Growth on the Stable Elastic-Plastic Fracture Mechanics, Engineering Fracture Mechanics, 77, pp. 2451-2466.
[44] Zaiser, M.; Grasset, F.M.; Koutsos, V.; Aifantis, E.C. (2004) Self-Affine Surface Morphology of Plastically Deformed Metals, Phys. Rev. Lett. 93: 195507.
[45] Weiss, J. (2001) Self-Affinity of Fracture Surfaces and Implications on a Possible Size Effect on Fracture Energy. International Journal of Fracture. 109: 365–381.
[46] Mishnaevsky Jr, L. (2000) Optimization of the Microstructure of Ledeburitic Tool Steels: a Fractal Approach. Werkstoffkolloquium (MPA, University of Stuttgart).
[47] Fung, Y.C. (1969) A first course in continuum mechanics. N. J: Prentice-Hall, INC, Englewood Criffs.
[48] Holian, B.L.; Blumenfeld, R.; Gumbsch, P. (1997) An Einstein Model of Brittle Crack Propagation. Phys. Rev. Lett. 78: 78–81, DOI: 10.1103/PhysRevLett.78.78.

[49] Herrmann, H.J., Kertész, J.; De Arcangelis, L. (1989) Fractal Shapes of Deterministic Cracks, Europhys. Lett. 10(2): 147-152.